Available at
http://pvamu.edu/aam
Appl. Appl. Math.
ISSN: 1932-9466

Applications and Applied Mathematics:
An International Journal
(AAM)

Vol. 14, Issue 1 (June 2019), pp. 296 – 311

Two Dimensional Mathematical Study of Flow Dynamics Through Emphysemic Lung

[1] **Jyoti Kori and** [2] **Pratibha**

Department of Mathematics
Indian Institute of Technology Roorkee
Roorkee -247667
Uttarakhand, India
[1]jyotikorii@gmail.com; [2]pratifma@iitr.ac.in

Received: July 29, 2018; Accepted: December 31, 2018

Abstract

There are various lung diseases, such as chronic obstructive pulmonary disease, asthma, fibrosis, emphysema etc., occurred due to deposition of different shape and size particles. Among them we focused on flow dynamics of viscous air through an emphysemic lung. We considered lung as a porous medium and porosity is a function of tidal volume. Two dimensional generalized equation of momentum is used to study the flow of air and equation of motion is used to study the flow of nanoparticles of elongated shape. Darcy term for flow in porous media and shape factor for nonspherical nanoparticles are used in mathematical model. Finite difference technique is used to solve the governing equation numerically. Various parameters such as inlet Reynolds number, media porosity, Darcy number, breathing rate and particle shape factor are found on flow dynamics. Results demonstrated that during inhalation, breathing stress increases and the deposition of particles is smaller due to the rupture alveoli in an emphysematous lung as compared to healthy lung.

Keywords: Emphysema; Elongated shape; Lung disease; Particle shape; Particle deposition; Porous media; Pulsatile flow

MSC 2010 No.: 35Q35, 37N10, 58D30, 76A02

1. Introduction

Emphysema and chronic bronchitis are two conditions gathered under the more broad term, chronic obstructive pulmonary disease (COPD). Emphysema causes the air sacs in lungs to rupture and lessen the surface area of the lungs, which gradually makes the respiration difficult. Earlier there was no antidote for emphysema, but now medicines such as bronchodilators are available as inhalers in both metered dose form and powder inhaler. The main cause of emphysema is long-term exposure to airborne irritants and pollutants, such as tobacco smoke, air pollution, chemical fumes, manufacturing fumes and cooking fires. It is believed that the most airborne particles were derived from fossil, biomass, and solid fuels combustion [Cheng et al. (2014)]. Epidemiological studies have confirmed that air pollution makes adverse health effects, especially if the pollutant is in nanoscale [Tang et al. (2014)]. Thus, nowadays most attention paid to airborne pollutants lies in nanoparticles and ultrafine particles.

By definition, nanoparticles are characterized by particle dimensions not exceeding 100 nm [Maynard (2007)]. Nanoparticles form a subcategory of ultrafine particles, which have some physical properties such as shape and orientation that make them different from spherical particles. Shape factor allows long skinny nanoparticles to orient with the smallest diameter within the direction of air flow (align along their long axis) and permitting them to deposit deep inside the lung airways [Timbrell (1982)]. A study by Geng et al. (2007) showed that nonspherical particles have higher chances of survival during the circulation in the vascular system as compared to spherical ones. Due to their small size, they are able to penetrate the lung epithelium and enter the blood circulation within a rather short time span [Geiser et al. (2005)]. Sturm and Hofmann [Sturm (2004)] presented a numerical model for particle deposition by the combined mechanisms of sedimentation and diffusion using various models of emphysema, for 0.001 to 10 μ m particles from generations 12th to alveoli and found particle deposition was shown to be higher in the healthy model compared to models representing various types of emphysema.

Also, it has been seen in some theoretical work that wall motion is a vital element because it drives alveolar flow [Balashazy et al. (2008)]. Tsuda et al. (1985) first reported the effect of tidal breathing on particle deposition in an alveolated duct model. They demonstrated that tidal breathing in a rhythmically moving alveolated duct geometry would lead to highly complex and irreversible flows and perceivable particle mixing and dispersion. Tippe and Tippe (2000) experimentally studied a scale-up model of a rhythmically expanding and contracting alveolus mounted on a straight duct with steady and unidirectional flow through the duct. They found that the flow features changed dramatically due to the presence of rhythmic wall motion. Girish et al. (2018) studied laminar natural convection in the vertical double-passage porous annuli, while same study done by Sankar (2018) in the presence of viscous dissipation and magnetic field. Further Sankar et al. (2018) studied laminar natural double diffusive convection in an open ended vertical cylindrical annulus with unheated entry and unheated exit. A most recent study by Amit et al. (2017) discovered that septal destruction lowers the flow resistance through the alveolar ducts and has little influence on the mass transport of oxygen into the alveoli.

In literature, most of studies are based on the flow behavior in an emphysema affected lung by considering rupture in septal wall and some studies are centered on the deposition of spherical

particles in an emphysema affected lung. No attention has been paid to the porous characteristic of emphysematous lungs together with particle shape impact on the deposition. These fundamental facts are still very poorly understood. Therefore, it is our purpose to fill this gap. In our study, fluid flow is examined in the two-dimensional, emphysemic and healthy alveolar sac model geometries with pulsatile flow of fluid under rhythmic breathing condition. The generalized Navier Stokes equation for a porous media are used to describe the flow condition for an emphysema affected lung. Also, the Newton second equation of motion is used for particle trajectory with particle shape factor. Effects of $1 \leq$ Reynolds number ≤ 30, $3 \leq$ aspect ratio ≤ 1000 and $12 \leq$ breathing rate ≤ 30 are considered. Lastly, the stress due to emphysema verses normal lung analyzed by stress/axial distance graph.

2. Mathematical Model

To understand the flow regime within the alveolar region, an extended horizontal cylindrical tube with radius r hooked up a single alveolus of diameter d_i placed perpendicular to the incoming oscillatory flow in Y-direction is taken into account [Balashazy et al. (2008)]. The impedance effect generated by emphysema lung is simulated by Darcy regime. A schematic of the problem is shown in Figure 1. Y is axial direction of flow while X is radial direction of flow. We assume that the fluid is Newtonian, viscous with constant density and flow is fully developed, unsteady and laminar. The conservation equations together with mass, momentum and kinematic equations for wall deformation in the cylindrical coordinates system (x, y, z) are given as follows:

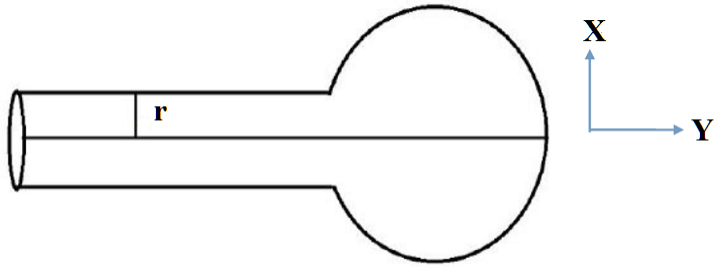

Figure 1. Schematic diagram of alveolar duct attached with single alveoli.

2.1. Governing Equations

Equation of continuity,

$$\frac{\partial u_x}{\partial x} + \frac{u_x}{x} + \frac{\partial u_y}{\partial y} = 0, \tag{1}$$

$$\frac{\partial v_x}{\partial x} + \frac{v_x}{x} + \frac{\partial v_y}{\partial y} = 0. \tag{2}$$

Equation of radial momentum,

$$\frac{\partial u_x}{\partial t}+\frac{u_x}{\epsilon}\frac{\partial u_x}{\partial x}+\frac{u_y}{\epsilon}\frac{\partial u_x}{\partial y}=-\frac{\epsilon}{\rho_a}\frac{\partial p}{\partial x}+\nu\left(\frac{\partial^2 u_x}{\partial x^2}+\frac{1}{x}\frac{\partial u_x}{\partial x}+\frac{\partial^2 u_x}{\partial y^2}\right)+\left(-\frac{\epsilon\nu}{K}u_x+k_f\frac{\rho_p}{\rho_a}\left(v_x-u_x\right)\right), \tag{3}$$

Equation of axial momentum,

$$\frac{\partial u_y}{\partial t}+\frac{u_x}{\epsilon}\frac{\partial u_y}{\partial x}+\frac{u_y}{\epsilon}\frac{\partial u_y}{\partial y}=-\frac{\epsilon}{\rho_a}\frac{\partial p}{\partial y}+\nu\left(\frac{\partial^2 u_y}{\partial x^2}+\frac{1}{x}\frac{\partial u_y}{\partial x}+\frac{\partial^2 u_y}{\partial y^2}\right)+\left(-\frac{\epsilon\nu}{K}u_y+k_f\frac{\rho_p}{\rho_a}\left(v_y-u_y\right)\right). \tag{4}$$

K is permeability and depends on the porosity ϵ [Khanafer et al. (2012)] as follows:

$$K=\frac{\epsilon^3 d_p^2}{150\left(1-\epsilon\right)^2}. \tag{5}$$

The lung volume at the maximum inspiration level is the total lung capacity (TLC) for use emphysemic lung. Tidal volume decrease because the patient is not able to inhale and exhale normally. The victims lungs are expanded and fills the chest before required volume of air can be inhaled. When the victim exhales, he is not able to fully do so because of the higher residual volume in his lungs. Therefore, we can find the porosity of a lung in terms of tidal volume as follows:

$$\textit{Porosity}(\epsilon)=\frac{\textit{Tidal lung volume}(v_t)}{\textit{Total Volume}(V)}. \tag{6}$$

The equation of motion for the particle trajectory in the radial direction is

$$\frac{\partial v_x}{\partial t}+v_y\frac{\partial v_x}{\partial y}+v_x\frac{\partial v_x}{\partial x}=\frac{F_{d_1}}{m}, \tag{7}$$

where, F_{d_1} is drag force on spherical particle and m is mass of particle.

The equation of motion for the particle trajectory in axial direction is

$$\frac{\partial v_y}{\partial t}+v_y\frac{\partial v_y}{\partial y}+v_x\frac{\partial v_y}{\partial x}=\frac{F_d}{m}. \tag{8}$$

Different particle shapes will make different drag forces and different particle terminal settling velocities, which might successively have an effect on the aerodynamic behavior of the particles

[Crowder et al. (2002)]. A term known as particle shape factor (S_f) [Fuchs (1994)] is employed to figure out the transport and deposition of non spherical particles. This factor simply describes the proportion of drag force on the non spherical nano particles (F_d) and (F_{d_1}) to the corresponding drag force on the related spherical particles with an equivalent volume [Hinds (1999)]. Mathematically, this relationship is expressed as

$$\begin{aligned} F_d &= S_f f_d, \\ F_{d_1} &= S_f f_{d_1}. \end{aligned} \tag{9}$$

Stokes drag forces are defined as

$$\left.\begin{aligned} f_d &= k_f\left(u_y - v_y\right) \\ f_{d_1} &= k_f\left(u_x - v_x\right) \end{aligned}\right\} \quad \text{where,} \quad k_f = 3\pi\mu C_f d_p, \tag{10}$$

$$C_f = 1 - \frac{\lambda}{d_p}\left[2.514 + 0.800\exp\left(\frac{-0.55.d_p}{\lambda}\right)\right], \qquad \lambda = 0.066\mu m. \tag{11}$$

The individual particle shape factor (S_f) is obtained from

$$S_f = \frac{1}{3}\left(\frac{2}{S_\parallel} + \frac{1}{S_\perp}\right), \tag{12}$$

where, C_f represents the Cunningham slip correction factor for thin particles and d_p is the diameter of elongated nano particle that depends upon the particle shape factor. Computation of the particle shape factor does not solely depends on particle geometry, but is additionally determined by the coordination of a particle relative to the direction of air flow. A straightforward empirical idea for the dependency of S_f on particle coordination was popularized by Su and Cheng [Su and Cheng (2006)]. The authors described $S_\perp$ for those particles that are adjusted with their long axes (upright to the air stream) and $S_\parallel$ for those whose long axes are aligned parallel to the air stream. Mathematically, $S_\perp$ and $S_\parallel$ are given by

$$\left.\begin{aligned} S_\perp &= \frac{\frac{8}{3}\left(\beta^2-1\right)\beta^{\frac{-1}{3}}}{\left(\frac{(2\beta^2-3)}{(\beta^2-1)^{\frac{1}{2}}}\right)\ln\left(\beta+(\beta^2-1)^{\frac{1}{2}}\right)+\beta} \\ S_\parallel &= \frac{\frac{4}{3}\left(\beta^2-1\right)\beta^{-\frac{1}{3}}}{\left(\frac{(2\beta^2-1)}{(\beta^2-1)^{\frac{1}{2}}}\right)\ln\left(\beta+(\beta^2-1)^{\frac{1}{2}}\right)-\beta} \end{aligned}\right\} \quad \beta > 1, \tag{13}$$

where β denotes the aspect ratio (the quantitative relation of particle length to particle width). The mathematical formulation of the aerodynamic diameter [Fuchs (1994)] simplifies to

$$d_p = d\left(\frac{\rho_p}{S_f\rho_0}\right)^{\frac{1}{2}}, \tag{14}$$

where ρ_0 is unit density, ρ_p is density of particle and d ia diameter of spherical particles.

Due to the deformation of alveolus wall and right heart pressure there is a time dependent pressure gradient within the alveolus given by

$$-\frac{\partial p}{\partial y} = \exp(-\alpha' tr/U_0) + S_f. \tag{15}$$

2.2. Initial and Boundary Conditions

The following initial and boundary conditions at $t = 0$ are used in the study:

1. At rest, no flow takes places therefore

$$u_x = v_x = u_y = v_y = 0. \tag{16}$$

2. We assume there is no radial flow along the axis of the alveolar tube so the axial velocity gradient adequate to zero

$$u_x = 0, v_x = 0, \frac{\partial u_y}{\partial x} = 0, \frac{\partial v_y}{\partial x} = 0. \tag{17}$$

3. The no-slip condition is forced at the inner surface of the wall.

3. Mathematical Solution

3.1. Transformation of the Governing Flow Equations

$$X^* = \frac{x}{r}, Y^* = \frac{y}{r}, p^* = \frac{P}{\rho_a U_0^2}, \tau^* = \frac{t}{t_0}, U_x^* = \frac{u_x}{U_0}, U_y^* = \frac{u_y}{U_0}, V_x^* = \frac{v_x}{U_o},$$
$$V_y^* = \frac{v_y}{U_o}, D_a = \frac{K}{r^2}, P_l = \frac{\rho_p}{\rho_a}, S_m = \frac{rk}{U_0}, Re = \frac{rU_0}{\nu}, S = \frac{r}{U_0 t_0}, \tag{18}$$

where, r is the radius of circular tube, t_0 initial time, U_0 initial velocity, Re is the Reynolds number and the S_t is the Strouhal number. By using the above quantities, together with our assumptions, we got the following dimension less equations in axial direction,

$$\frac{\partial U_x}{\partial X} + \frac{U_x}{X} + \frac{\partial U_y}{\partial Y} = 0. \tag{19}$$

$$\frac{\partial V_x}{\partial X} + \frac{V_x}{X} + \frac{\partial V_y}{\partial Y} = 0. \tag{20}$$

$$S_t \frac{\partial U_y}{\partial \tau} + \frac{U_x}{\epsilon}\frac{\partial U_y}{\partial X} + \frac{U_y}{\epsilon}\frac{\partial U_y}{\partial Y} = -\epsilon \frac{\partial P}{\partial Y} + \frac{1}{R_e}\left(\frac{\partial^2 U_y}{\partial X^2} + \frac{1}{X}\frac{\partial U_y}{\partial X} + \frac{\partial^2 U_y}{\partial Y^2}\right)$$
$$+ S_m P_l (V_y - U_y) - \frac{\epsilon}{DaR_e} U_y. \tag{21}$$

$$S_t \frac{\partial V_y}{\partial \tau} + V_x \frac{\partial V_y}{\partial X} + V_y \frac{\partial V_y}{\partial Y} = \frac{S_f S_m \left(U_y - V_y\right)}{m}. \tag{22}$$

Transformed boundary conditions at $\tau = 0,\ \ U_x = 0, U_y = 0, V_x = 0, V_y = 0,$ (23)

at X=0, $U_x = 0, \frac{\partial U_y}{X} = 0, V_x = 0, \frac{\partial V_y}{X} = 0.$ (24)

at X=1, $U_x = 0, U_y = 0, V_x = 0, V_y = 0.$ (25)

The Womersley number is responsible for the frequency of the oscillatory flow. It is related to the Reynolds number and is defines as,

$$w_0 = \sqrt{2\pi ReSt}. \tag{26}$$

The stress due to an emphysema affected lungs given by,

$$T = \mu \left(\frac{\partial U_y}{\partial x} + \frac{\partial U_x}{\partial y} \right). \tag{27}$$

3.2. Numerical Analysis

Analytical approaches are suitable for linear problems. However, the presented governing equations are nonlinear and related to regular geometry. It is troublesome to find the solution of nonlinear equations subject to initial and boundary conditions by an analytical approach. Therefore, we have utilized a numerical procedure in an attempt to solve the nonlinear equations. Numerous numerical techniques, such as the, finite difference method (FDM) [Saini et al. (2017); Kori and Pratibha (2018); Kori and Pratibha (2019a); Kori and Pratibha (2019b); Kori and Pratibha (2019c); Saini et al. (2014); Saini et al. (2017)], finite element method [Fukushima et al. (1982)] and finite volume method [Guo et al. (1997); Lee et al. (2007)] have been used to solve the problem. FDM is a basic and less tedious technique for the regular geometry. Thus, to solve presented problem, we too applied a finite difference numerical scheme. The discretization of velocity $U(X, Y, \tau)$ is written as $U_y(X_i, Y_j, \tau_n)$ or $(U_y)^n_{i,j}$. We define

$$\begin{aligned} &X_i = i\Delta x,\ \ i = 0, 1, 2, 3, 4, ..., N,\ \ \text{where,}\ \ r_N = 1. \\ &Y_j = j\Delta y,\ \ j = 0, 1, 2, 3, 4, ..., M, \\ &\tau_n = (n-1)\Delta\tau,\ \ n = 1, 2, ... \end{aligned} \tag{28}$$

i, j and n are radial, axial and time index. $\Delta X, \Delta Y$ and $\Delta\tau$ are the increment in radial, axial directions and time respectively. We used central difference approximations, for all the spatial derivatives, as follows:

$$\frac{\partial U_y}{\partial Y} = \frac{(U_y)^n_{i,j+1} - (U_y)^n_{i,j-1}}{2\Delta Y}. \tag{29}$$

For the second order central difference approximation for time and space derivatives, we used:

$$\frac{\partial^2 U_y}{\partial Y^2} = \frac{(U_y)^n_{i,j+1} - 2(U_y)^n_{i,j} + (U_y)^n_{i,j-1}}{(\Delta Y)^2}. \tag{30}$$

and for the first order time derivative at point (X_i, Y_j, τ_n), we applied the forward difference approximation as follows:

$$\frac{\partial (U_y)}{\partial \tau} = \frac{(U_y)^{n+1}_{i,j} - (U_y)^n_{i,j}}{2\Delta\tau}. \tag{31}$$

Grid independence of the solution is also checked for various grid sizes, 70x70, 80x80, and 100x100 in the axial and radial directions. We found that the results remain consistent when the grid size is set to 100x100, when the time step was chosen to be $\Delta\tau = 0.001$, $\Delta X = 0.01$ and $\Delta Y = 0.01$ along the radial and axial directions, respectively. The grid mesh is uniform in both directions.

3.3. Computational Stability

To determine the air (U_y) and particle (V_y) velocities, the above equations are solved explicitly by using the defined discretization techniques with the following stability criteria

$$max\{\frac{\Delta\tau}{\Delta X^2}\} \leq 0.5. \tag{32}$$

Results are appeared to converge with the accuracy of order 10^{-3}.

4. Results and Discussions

The two-point boundary value problem, defined by Equations (18) - (27), is controlled by Reynolds number (Re), Strouhal number (S_t), Womersley number (α), Darcy number (Da), Aspect ratio (β), Breathing rate (α') and Porosity (ϵ). Additionally, the effect of the disease can be seen by a comparison between a normal lung and an emphysema affected lung. To calculate effect of the above parameters, the numerical values defined in Table 1 are used [Haefeli-Bleuer and Weibel (1988); Saini et al. (2017); Weibel (1964)].

Table 1. Numerical values used in the study

Variable	Value	Variable	Value
m	0.0002 Kg/l	d	100 nm
f_p	1.2 hz	ρ_a	1.145 kg/m^3
ρ_p	0.02504*$10^{12}/m^3$	r	125 μ m
a_2	0.5 Kg/m^2s^2	ν	1.71*$10^{-5}m^2/s$
u_{in}	0.3 m/s		

4.1. Importance of Aspect Ratio (β)

The aspect ratio (β) is defined as the ratio of particle length to particle width. In the environment, not all particles are perfectly spherical in shape, hence to keep account of nonspherical nanoparticles, aspect ratio is a key factor. We used elongated nanoparticles from aspect ratio $3 \leq \beta \leq 1000$, which covers a wide range of an inhalable nonspherical nanoparticles [Sturm and Hofmann (2009)] and compare our result with Saini et al. (2017) at Re=10, d=100nm and ϵ=0.84.

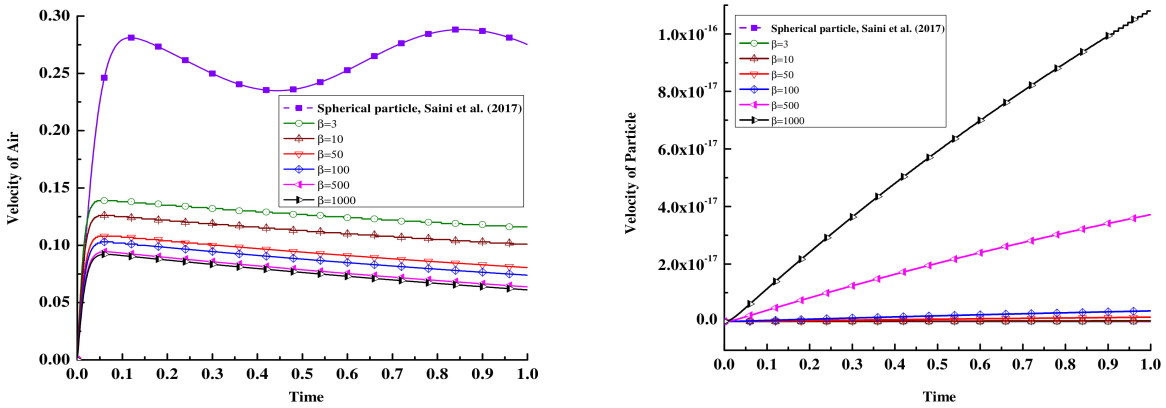

(a) (b)

Figure 2. Effect of spherical and nonspherical nanoparticles ($3 \leq \beta \leq 1000$) on the axial velocity of (a) air and (b) particle at Re=10, d=100nm and ϵ=0.84.

We found that the axial velocity of a particle (V_y), in Figure 2(a), is very low for spherical nanoparticles [Saini et al. (2017)] and it increases due to increment in the aspect ratio from 3 to 1000. While, axial velocity of air, in Figure 2(b), is high for spherical nanoparticles and it decreases due to increment in aspect ratio from 3 to 1000. From these Figure we observe that the high aspect ratio particle applies high drag force on the air stream therefore, velocity of air become low, however, spherical particle or low aspect ratio particle applies low drag force on the air stream and hence, velocity of air become high.

4.2. Effect of Reynolds Number (Re)

In Figure 3, we show effects of the Reynold number (from 10 to 30) at $\beta = 10$, d=100nm and ϵ=0.84 on the axial velocity of air and particles. From Figure 3(a), we found by increasing the Reynold number from 10 to 30, axial velocity of air U_y increases gradually with time. Also, from Figure 3(b), we found by increasing the Reynold number from 10 to 30, axial velocity of particle V_y increases with time. Since, large Reynold number results with thinner concentration boundary layer on the walls of airways, which promotes overall gas transfer while, low Reynolds number causes high concentration on the walls of airways. Therefore, at Reynold number =30, the viscosity of fluid reduced than at Reynold number =10 which cause increment in the flow of fluid.

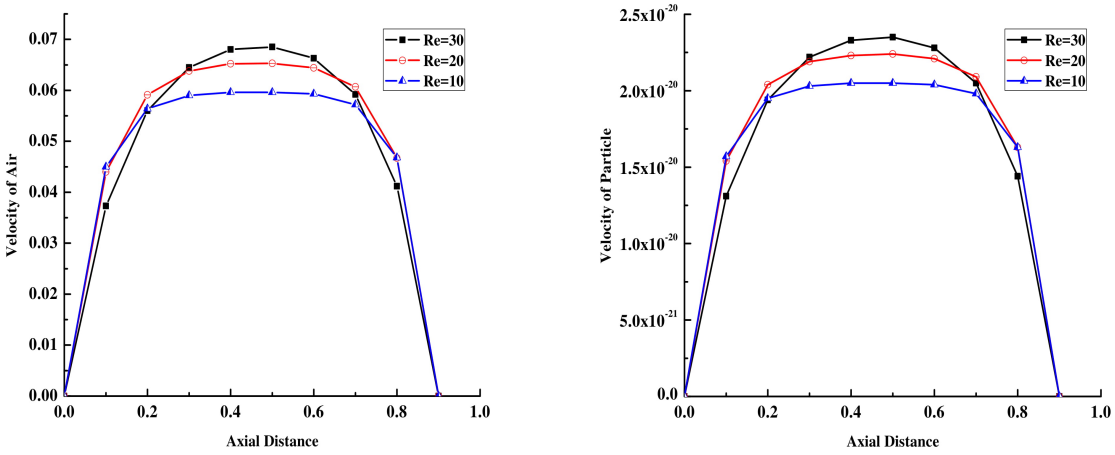

(a) (b)

Figure 3. Effect of Reynolds number on the axial velocity of (a) air U_y and (b) particle V_y at β=10, d=100nm and ϵ=0.84.

4.3. Effect of Porosity (ϵ)

In Figure 4, we show the effects of porosity ϵ for a normal to an emphysema lung. We used porosity as a function of tidal volume to find the impact of emphysema on the axial velocity of air and particles at β=10, d=100nm and Re=10.

From Figure 4(a)-4(b), we found that for an emphysema and a normal lung the axial velocity of air U_y and particle V_y increases gradually with time. While, the velocities for a normal lung is less than an emphysema affected lung. Since large pore size or highly permeable medium allow fluid to pass easily. Therefore, an emphysema affected lung allow flow of air easily comparative to a normal lung but physiologically this behavior of an emphysema affected lung create problem in cyclic breathing.

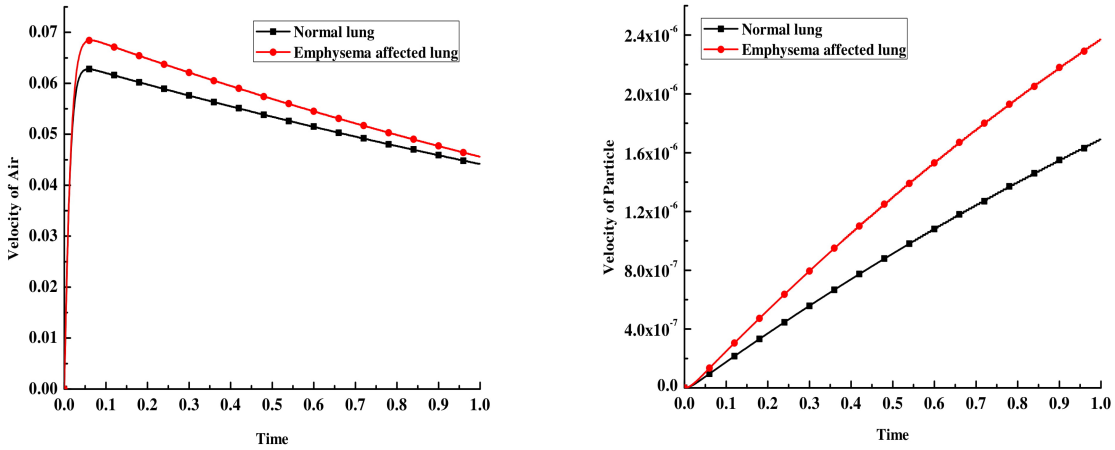

(a) (b)

Figure 4. Effect of porosity on the axial velocity of (a) air U_y and (b) particle V_y at β=10, d=100nm and Re=10

4.4. Effect of Darcy Number (Da)

In Figure 5, we can see the effect of the Darcy number on flow regime at β=10, d=100nm, ϵ=0.84 and Re=10. We found that by decreasing the value of the Darcy number from 0.01 to 0.001, air U_y and particle V_y velocities (in Figure 5(a)-5(b)) due to an emphysema, increased gradually with time. Since, the flow through highly porous media applied low drag force on fluid and also the pressure gradient on the flow become less, therefore, velocity of fluid increases with respect to time by decreasing the Darcy number. From this result we can concluded that the highly porous media allow the air flow more freely.

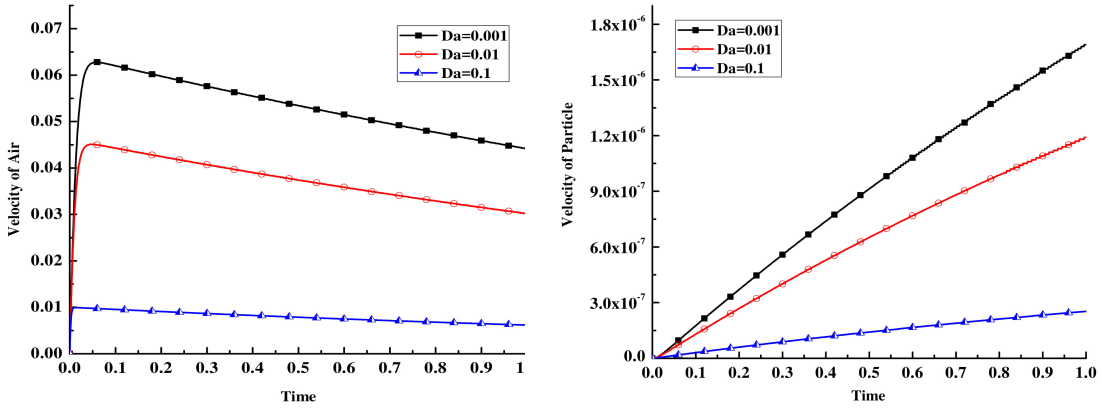

(a) (b)

Figure 5. Effect of Darcy number on the axial velocity of (a) air U_y and (b) particle V_y at β=10, d=100nm, ϵ=0.84 and Re=10.

4.5. Effect of Breathing Rate (α')

In Figure 6, we found the effect of breathing rate α' from 12 to 30 breath per minute on the velocity of axial air U_y and particles V_y at β=10, d=100nm, ϵ=0.84 and Re=10.

We found for normal breath (α'=12), velocity of air (in Figure 6(a)) and particle (in Figure 6(b)) first increase upto the axial distance Y = 0.5 and then it decreases with the axial distance down to zero velocity but as we increase breathing rate by considering an emphysema disease, we got decrement in velocity of air and particle. Hence, we can concluded from this Figure that for an emphysema affected lung patient is not able to breath properly.

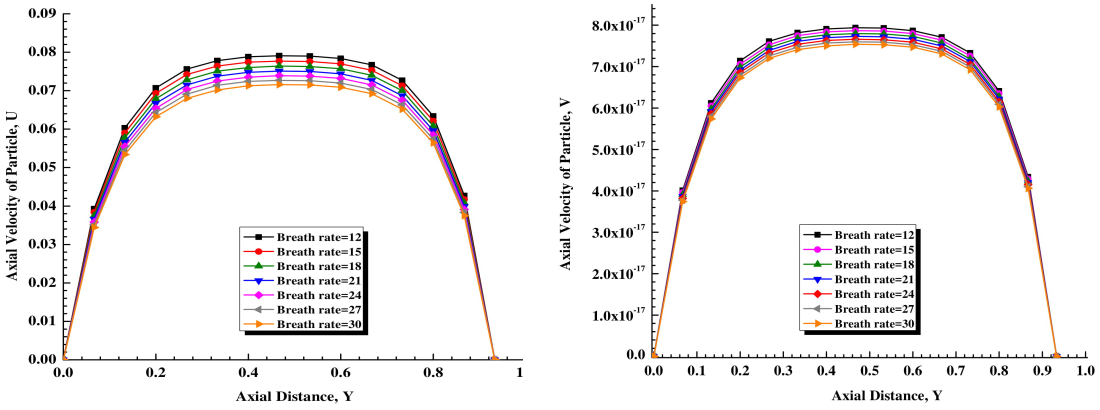

(a) (b)

Figure 6. Effect of breathing rate on the axial velocity of (a) air U_y and (b) particle V_y at β=10, Re=5.

4.6. Effect of Emphysema on Breathing

A typical breathing stress/axial distance relationship for inhalation and exhalation is given in Figure 7. Inspiration is an active process; the contraction of the diaphragm and the external intercostal muscles expand the tissue matrix supporting the airways, inflating them and generating the suction pressure required to force air into the lung. As the air flows into the lungs, the pressure equalizes with the atmosphere, until there is no more flow, which signals the end of inspiration. Figure 7 shows that the inspiratory breathing stress dependence on axial distance can be approximated as a sinusoidal. Normal exhalation by contrast is a passive process; as the intercostal muscles relax, the natural elasticity of the lung parenchymal tissues serve to recoil the nonspherical nanoparticle attached to the airways, compressing them. This phenomenon is known as elastic recoil.

The breathing stress in Figure 7 (in Table 2) increases linearly with the axial distance, until it reaches maximum inspiration. Thereafter it falls linearly to zero and take pause during the elastic recoil, on axial distance=0.5. It then starts decreasing and signaling the end of expiration at axial distance=0. Emphysematous degradation of the tissue matrix supporting the airways leads to the loss of elastic recoil of the lung parenchyma. As a result, airways do not inflate as effectively and the maximum inspiratory flow rate and volume excursion at the end of inspiration is reduced. Due

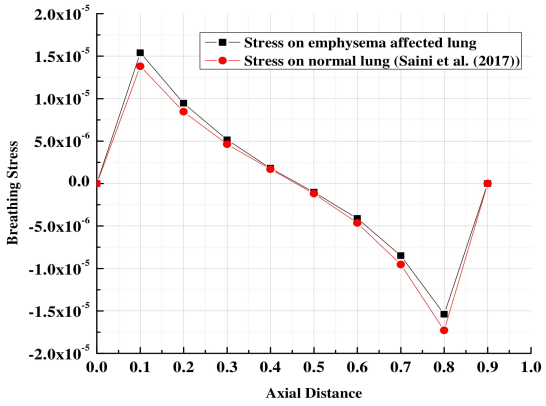

Figure 7. Variation of breathing stress versus axial distance for healthy and emphysema affected lungs.

Table 2. Effect of emphysema on breathing

Axial distance	Stress on emphysema affected lung	Stress on normal lung
0	0	0
0.1	1.54E-5	1.38E-5
0.2	9.45E-6	8.46E-6
0.3	5.13E-6	4.63E-6
0.4	1.81E-6	1.67E-6
0.5	-1.02E-6	-1.19E-6
0.6	-4.12E-6	-4.64E-6
0.7	-8.49E-6	-9.54E-6
0.8	-1.54E-5	-1.73E-5
0.9	0	0

to the decreased elastic recoil, the expiratory flow rate is also reduced. This reduction in flow rate due to emphysema is modelled by assuming lung is a porous media and porosity is a function of lung volume altering the volume for healthy and emphysema affected lung. The progression of the di1sease is accompanied by a reduction in fluid motion and fall in the inlet Reynolds number.

5. Conclusions

The effects of early stage emphysema on particle deposition and flow mechanics cannot be determined in vivo. As a result, numerical simulations are required to study the airflow in the lung under emphysematous conditions. The computational geometry utilized in this study spans one generation of alveolar duct attach with an alveoli. The effects of emphysema consists of destruction of alveolar septa and reduction in airway flow rate at the inlets of the computational domain. The gradual progression of these effects was investigated by comparing the results of a healthy case with diseased cases. The concluding remarks are as follows.

(1) Demonstrated that particle deposition is smaller in emphysematous lung compared with healthy lungs and this, in turn means particle deposition will occur more quickly when lungs

are healthy.

(2) It is found that emphysema produces a decrease in the oxygen transported to the acinus. This is primarily due to the drop in generated pleural pressures which in turn lead to lower flow rates into the acinar branches.
(3) In contrast, septal degradation has a notable effect on flow through acinus, where loss of the alveolar septa tends to decreases the overall resistance to the flow, and hence larger flow rates are observed in the ducts.
(4) It is found that the overall air velocity can be significantly increased by increasing the aspect ratio, alveoli size, Reynolds number, porosity and breathing rate.
(5) Comparison between a normal to an emphysema affected lung show an increase in stress due to rupture of the alveoli during inhalation.

Finally, we found present results are compatible with published results [Saini et al. (2017)] and useful to study the physical condition of emphysema affected lung. Further, we can study the physical condition of emphysema affected lung by using three dimensional flow to analyse the problem more realistically.

Acknowledgment

The author, Jyoti Kori, is thankful to Ministry of Human Resource Development (Grant Code:-MHR-02-23-200-44) India for providing funds and support while writing this manuscript.

REFERENCES

Dutta, A.V., Vasilescu, D.M., Hogg, J.C., Phillion, A.B. and Brinkerhoff, J.R. (2017). Simulation of Airflow in an Idealized Emphysematous Human Acinus, J. Biomech. Eng., Vol. 140, No. 7, pp. 071001.

Balashazy, I., Hofmann, W., Farkas, A. and Madas, B.G. (2008). Three-dimensional model for aerosol transport and deposition in expanding and contracting alveoli, Inha. Toxi., Vol. 20, pp. 611–621.

Cheng, Y., Engling, G., He, K., Duan, F., Du, Z., Ma, Y., Liang, L., Lu, Z., Liu, J., Zheng, M. and Weber, R.J. (2014). The characteristics of beijing aerosol during two distinct episodes: impacts of biomass burning and fireworks, Environmental Pollution, Vol. 185, pp. 149–157.

Crowder, T.M., Rosati, J.A., Schroeter, J.D., Hickey, A.J. and Martonen, T.B. (2002). Fundamental effects of particle morphology on lung delivery: predictions of Stokes' law and the particular relevance to dry powder inhaler formulation and development, Pharm. Res, Vol. 19, pp. 239–45.

Fuchs, N.A. (1994). *The Mechanics of Aerosols* New York: Pergamon Press.

Fukushima, T., Azuma, T., and Matsuzawa, T. (1982). Numerical Analysis of Blood Flow in the Vertebral Artery, J. Bio. Eng., Vol. 140, No 2, pp. 143–147.

Geiser, M., Rothen-Rutishauser, B., Kapp, N., Schürch, S., Kreyling, W., Schulz, H., Semmler, M., Hof, V.I., Heyder, J., and Gehr, P. (2005). Ultrafine particles cross cellular membranes by nonphagocytic mechanisms in lungs and in cultured cells, Environ Health Perspect, Vol. 113, pp. 1555–60.

Geng, Y., Dalhaimer, P., Cai, S., Tsai, R., and Tewari, M. (2007). Shape effects of filaments versus spherical particles in flow and drug delivery, Nature Nanotech., Vol. 2, pp. 249–55.

Girish, N., Makinde, O.D. and Sankar, M. (2018). Numerical Investigation of Developing Natural Convection in Vertical Double-Passage Porous Annuli, Defect and Diffusion Forum, Vol. 387, pp. 442–460.

Guo, Z., Kim, S., and Sung, H. (1997). Pulsating flow and heat transfer in a pipe partially filled with a porous medium, Int. J. Heat Mass Transfer, Vol. 40, pp. 4209–4218.

Haefeli-Bleuer, B. and Weibel, E.R. (1988). Morphometry of the human pulmonary acinus, The Anatomical Record, Vol. 220, pp. 401–411.

Hinds, W.C. (1999). Aerosol technology: Properties, behavior, and measurement of airborne particles, Springfield: Charles C Thomas Publisher, New York: John Wiley, pp. 249–89.

Khanafer, K., Cook, K., and Marafie, A. (2012). The role of porous Media in modeling fluid flow within hollow fiber membranes of the total artificial lung, J. Porous Media, Vol. 15, pp. 113–122.

Kori, J. and Pratibha. (2018). Numerical Simulation of Mucus Clearance inside Lung Airways, J Appl Fluid Mech, Vol. 11, No. 5, pp. 1163–1171.

Kori, J. and Pratibha. (2019a). Effect of Dynamic Shape Factor in Alveolar Region as a Filtration Media, World Journal of Modelling and Simulation, Vol. 14, No. 4.

Kori, J. and Pratibha. (2019b). Numerical Simulation of Dusty Air Flow and Particle Deposition Inside Permeable Alveolar Duct, Int. J. Appl. Comput. Math, Vol. 5, No. 17.

Kori, J. and Pratibha. (2019c). Simulation and modeling for aging and particle shape effect on airflow dynamics and filtration efficiency of human lung, J Appl Fluid Mech, Vol. 12, No. 4. pp. 1273– 285.

Lee, T., Liu, X., Li, G. and Low, H. (2007). Numerical Study on Sinusoidal Fluctuated Pulsatile Laminar Flow Through Various Constrictions, Commu. in compu. physics, Vol. 2, pp. 99–122.

Maynard, A.D. (2007). Nanotechnology: the next big thing, or much ado about nothing?, Ann. Occup. Hyg., Vol. 51, pp. 1–12.

Saini, A. and Katiyar, V.K. (2016). Two Dimensional Model of Pulsatile Flow of a Dusty Fluid through a Tube with Axisymmetric Constriction, World Journal of Modelling and Simulation, Vol. 12, No.1, pp. 70–78.

Saini, A., Katiyar, V.K. and Pratibha (2014). Effects of first-order chemical reactions on the dispersion coefficient associated with laminar flow through the lungs, International Journal of Biomathematics, Vol. 7, No. 2, pp. 1450021.

Saini, A., Katiyar, V., and Pratibha. (2017). Two-dimensional model of nanoparticle deposition in the alveolar ducts of the human lung, Appl. Appl. Math., Vol. 12, pp. 305–318.

Sankar, M. (2010). Numerical Study of Double Diffusive Convection in Partially Heated Vertical Open Ended Cylindrical Annulus, Adv. Appl. Math. Mech., Vol. 2, No. 6, pp. 763–783.

Sankar, M., Girish, N. and Siri, Z. (2018). Fully Developed Magnetoconvective Heat Transfer in Vertical Double-Passage Porous Annuli. In: Narayanan N., Mohanadhas B., Mangottiri

V. (eds) Flow and Transport in Subsurface Environment. Springer Transactions in Civil and Environmental Engineering. Springer, Singapore.

Smith, G. (1985). *Numerical Solution of Partial Differential Equations*, Oxford Univ. Press, Third Ed.

Sturm, R. and Hofmann W. (2004). Stochastic simulation of alveolar particle deposition in lungs affected by different types of emphysema, J Aerosol Med., Vol. 17, No. 4, pp. 357–372.

Sturm, R. and Hofmann, W., (2009). A Theoretical Approach to the Deposition and Clearance of Fibers With Variable Size in the Human Respiratory Tract, J. Hazard. Mater., Vol. 170, No. 1, pp. 210–218.

Su, W.C. and Cheng, Y.S. (2006). Deposition of Fiber in a Human Airway Replica, Aerosol Sci., Vol. 37, No. 11, pp. 1429–1441.

Tang, D., Li, T.Y., Chow, J.C., Kulkarni, S.U., Watson, J.G., Ho, S.S., Quan, Z.Y., Qu, L.R. and Perera, F. (2014). Air pollution effects on fetal and child development: a cohort comparison in China Environmental Pollution, Vol. 185, pp. 90–96.

Timbrell, V. (1982). Deposition and retention of fibres in the human lung, Ann. Occup. Hyg., Vol. 26, pp. 347–369.

Tippe, A. and Tsuda, A. (2000). Recirculating flow in an expanding alveolar model: Experimental evidence of flow-induced mixing of aerosols in the pulmonary acinus. Journal of Aerosol Science, Vol. 31, No. 8, pp. 979–986.

Tsuda, A., Henry, F.S., and Butler, J.P. (1985). Chaotic mixing of alveolated duct flow in rhythmically expanding pulmonary acinus, J Appl Physiol., Vol. 79, No. 3, pp. 1055–1063.

Weibel, E.R. (1964), Morphometrics of the Lung. Handbook of Applied Physiology, Am. Physiol. Soc., Vol 2, pp. 285–308.

Appendix

Nomenclature is defined in Table 3.

Table 3. Nomenclature

Variable	Description	Variable	Description
u_x	air velocity radial direction	v_x	particle velocity radial direction
u_y	particle velocity axial direction	v_y	particle velocity axial direction
t	stands for time	ϵ	for media porosity
ρ_p	density of particles	ρ_a	density of air
ν	kinematic viscosity	k_f	Stokes drag force
K	permeability of parenchyma	d_p	aerodynamic diameter
S_f	dynamic shape factor	C_f	correction factor
d	diameter of sphere of unite density	P_l	particle load
D_a	Darcy number	α'	breathing rate